Supporting Information

Iridium-based Nanowires as Highly Active, Oxygen Evolution Reaction Electrocatalysts

Shaun M. Alia*, Sarah Shulda, Chilan Ngo, Svitlana Pylypenko, and Bryan S. Pivovar

Dr. S. M. Alia, Dr. B. S. Pivovar
Chemistry and Nanoscience Center, National Renewable Energy Laboratory, 15013 Denver West Parkway, Golden, CO 80401, United States of America

S. Shulda, Dr. C. Ngo, Prof. S. Pylypenko
Department of Chemistry and Geochemistry, Colorado School of Mines, 1012 14th Street, Golden, CO 80401, United States of America

*Corresponding Author: Shaun M. Alia
Chemistry and Nanoscience Center, National Renewable Energy Laboratory
15013 Denver West Parkway, Golden, CO 80401, United States of America
E-mail: shaun.alia@nrel.gov

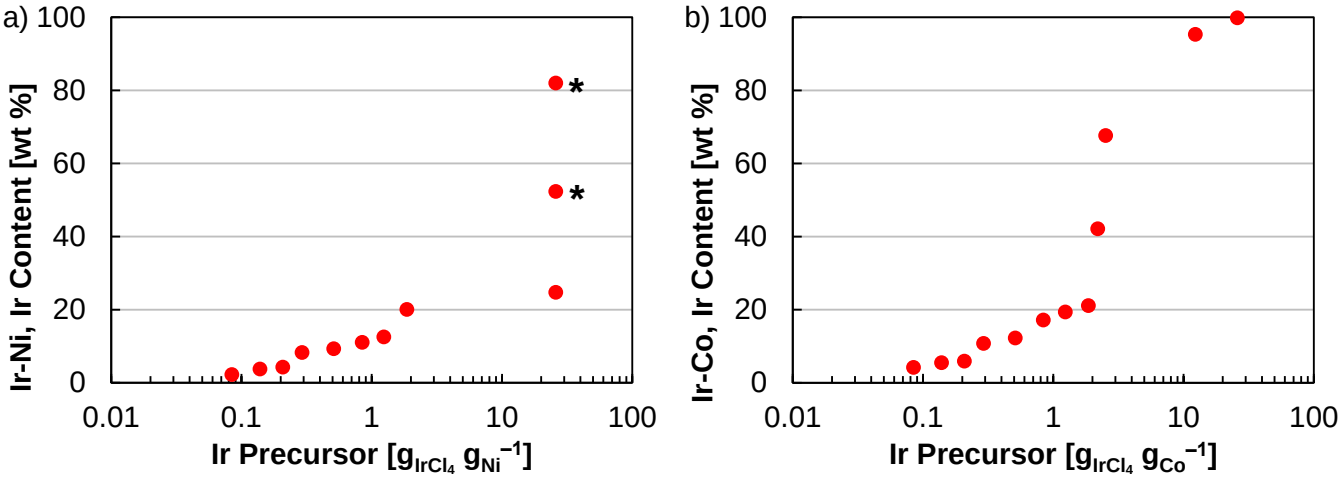

Figure S1. Displacement level (y-axis) as a function of the amount of Ir precursor (x-axis) for (a) Ir-Ni and (b) Ir-Co nanowires. Asterisks in (a) correspond to samples where increasing amounts of Ir chloride hydrochloric hydrate were added in place of Ir chloride hydrate.

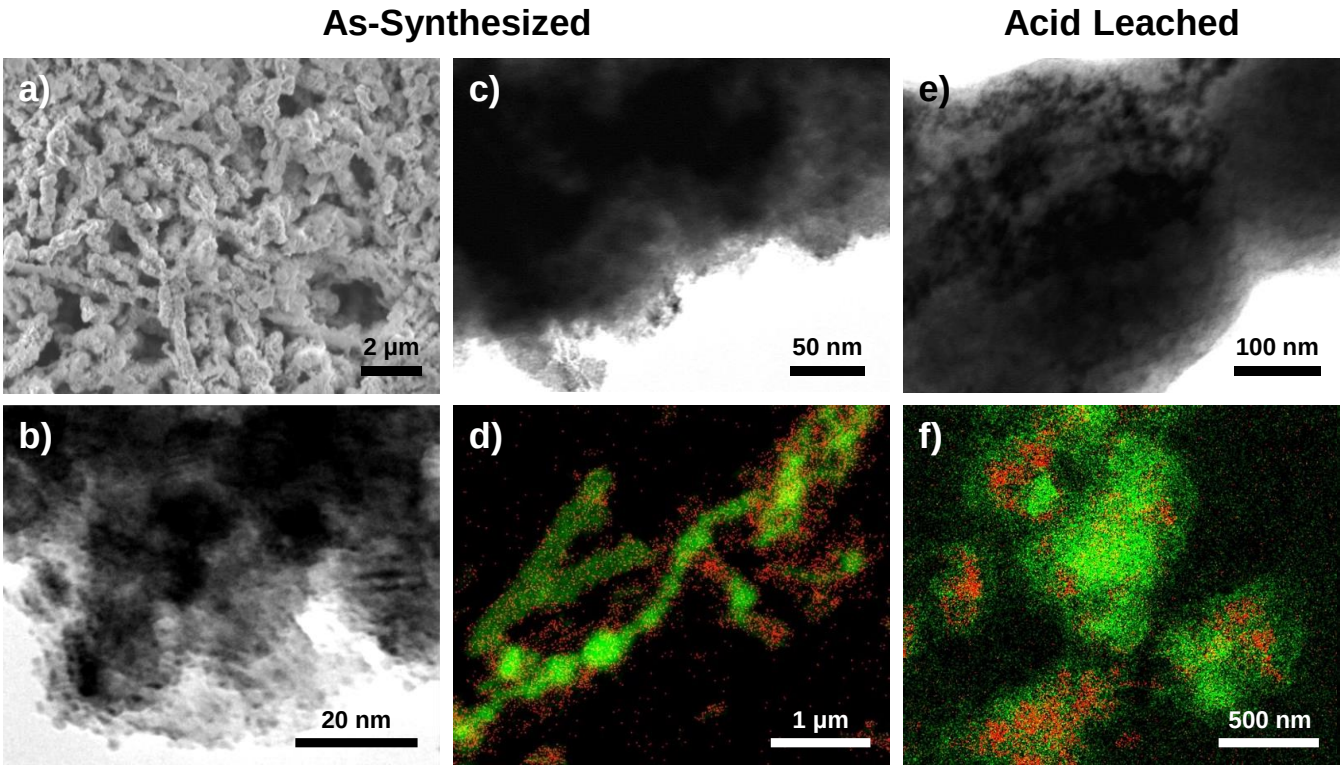

Figure S2. Microscopy and spectroscopy of Ir-Co nanowires, including (a-d) the as-synthesized nanowires (4.2 wt. % Ir) and (e-f) the acid leached nanowires (4.2 wt. % Ir as-synthesized, 93.6 wt. % Ir acid leached, (4.2) 93.6). EDS mapping shows elemental distribution for Ir (red) and Ni (green).

XRD Patterns:
Ir fcc peaks were found for (111) at 29.0°, (200) at 33.6°, (220) at 48.2°, and (311) at 57.1°.

Ni fcc peaks were found for (111) at 31.7°, (200) at 36.7°, and (220) at 52.8°.

Co fcc peaks were found for (111) at 31.5° and (220) at 52.4°; the peak for (200) at 36.5° was obscured and not marked in the figures. Co hcp peaks were found for (100) at 29.6° and (101) at 33.7°; the peak for (002) at 31.7° was not marked in the figures due to the higher prevalence of the Co fcc phase and its inference with the Co fcc (111) peak. Co_3O_4 monoclinic peaks were found for (220) at 22.4°, (311) at 26.4°, (511) at 41.8°, and (440) at 45.7°.

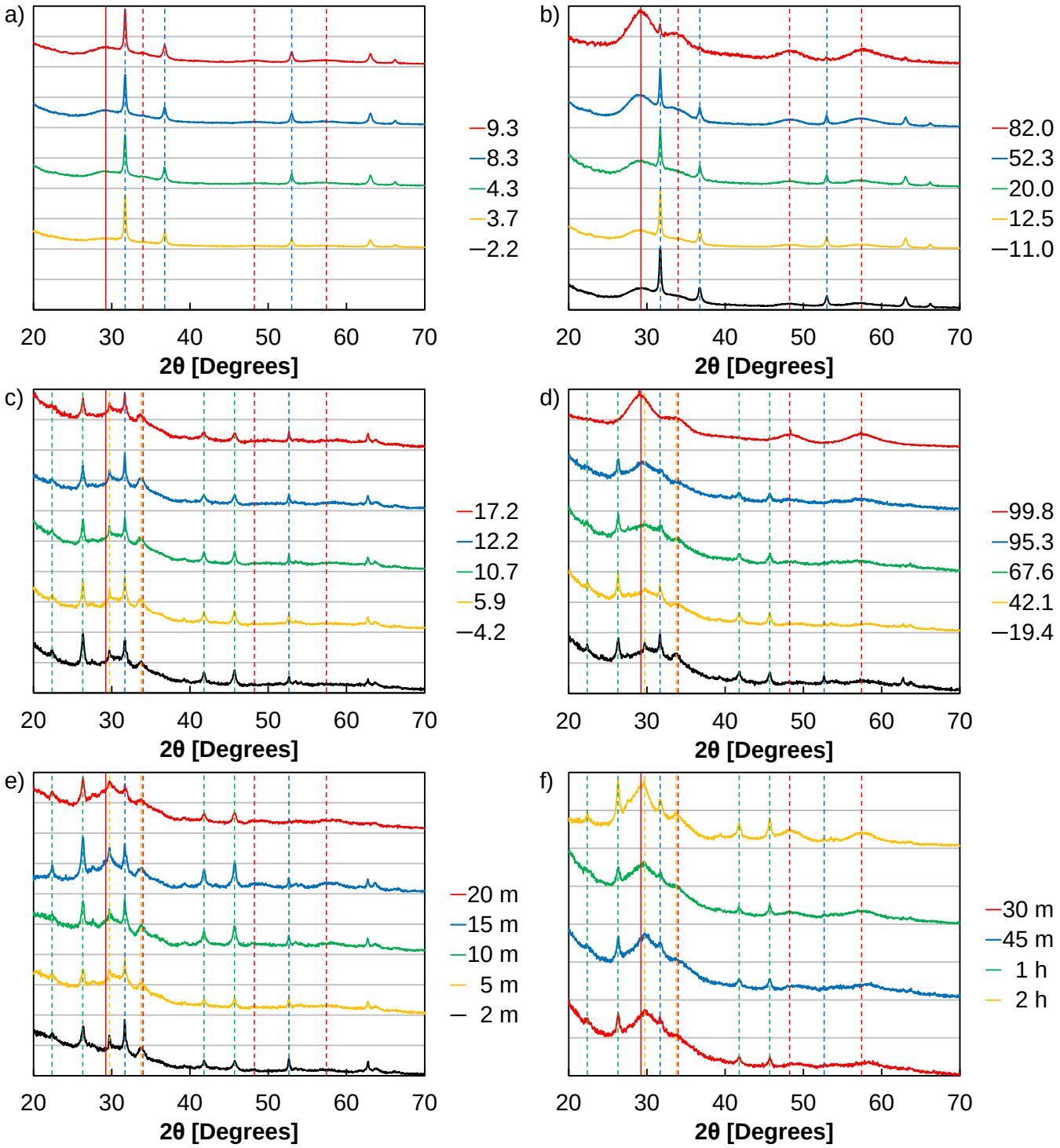

Figure S3. XRD patterns of the as-synthesized (a-b) Ir-Ni and (c-d) Ir-Co nanowires, with Ir composition (wt. % Ir) listed in the figure legends. (c-d) XRD snapshots during the formation of Ir-Co nanowires (42.1 wt. % Ir following synthesis), with synthesis time in minutes (m) and hours (h) listed in the figure legends. Vertical lines in (a-b) correspond to Ir fcc (red) and Ni fcc (blue). Vertical lines (c-f) correspond to Ir fcc (red), Co fcc (blue), Co_3O_4 monoclinic (green), and Co hcp (yellow). The solid red line (a-f) corresponds to the Ir fcc (111) peak. In figure subsets (e-f), Ir lattice compression appeared to occur initially during the displacement process. As displacement continued, the Ir fcc (111) peak shifted into the direction of a characteristically Ir lattice.

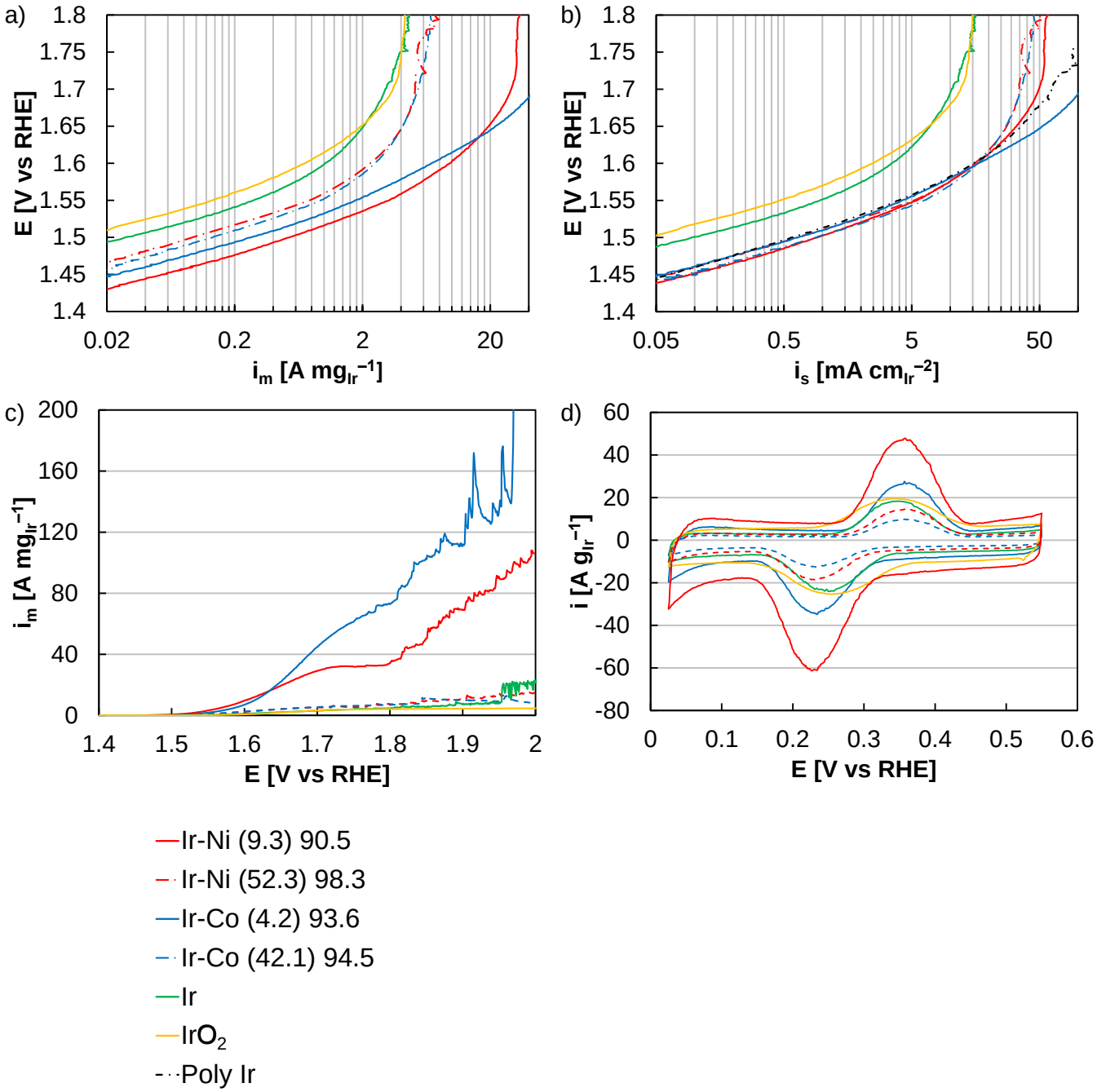

Figure S4. (a) Mass activity Tafel plots, (b) specific activity Tafel plots, (c) linear sweep voltammograms, and (d) mercury adsorption/desorption voltammograms of acid leached Ir-Ni and Ir-Co nanowires, Ir nanoparticles, Ir oxide nanoparticles (IrO_2), and polycrystalline Ir (Poly Ir). Activities were corrected for internal resistance and taken with a rotation speed of 2500 rpm and at a scan rate of 20 mV s^{-1} in a 0.1 M perchloric acid electrolyte. Mercury adsorption/desorption voltammograms were taken with a rotation speed of 1500 rpm and at a scan rate of 50 mV s^{-1} in a 0.1 M perchloric acid electrolyte containing 1 mM mercury nitrate.

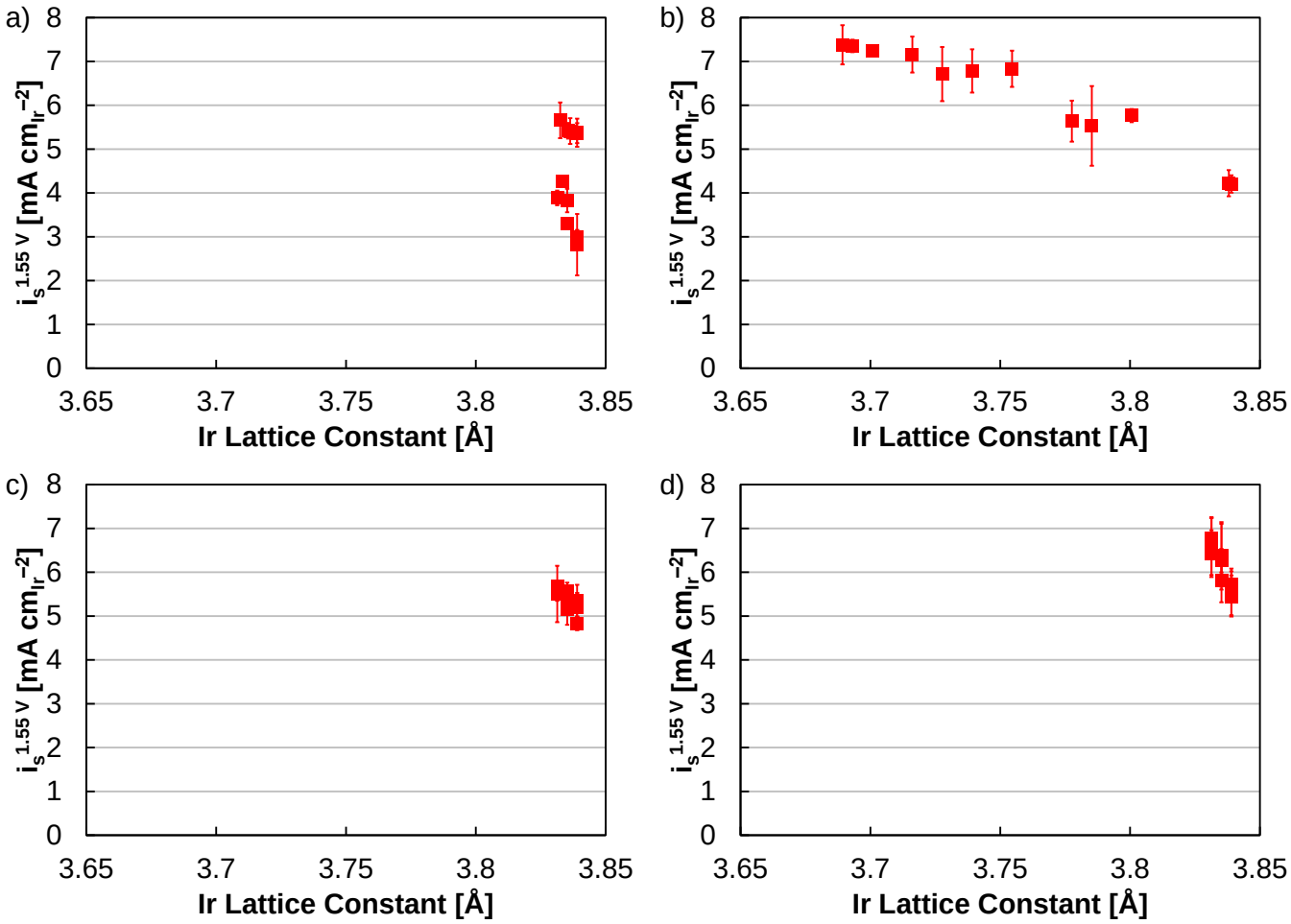

Figure S5. Specific OER activities of as-synthesized (a) Ir-Ni and (b) Ir-Co nanowires, and acid leached (c) Ir-Ni and (d) Ir-Co nanowires as a function of the Ir lattice constant.

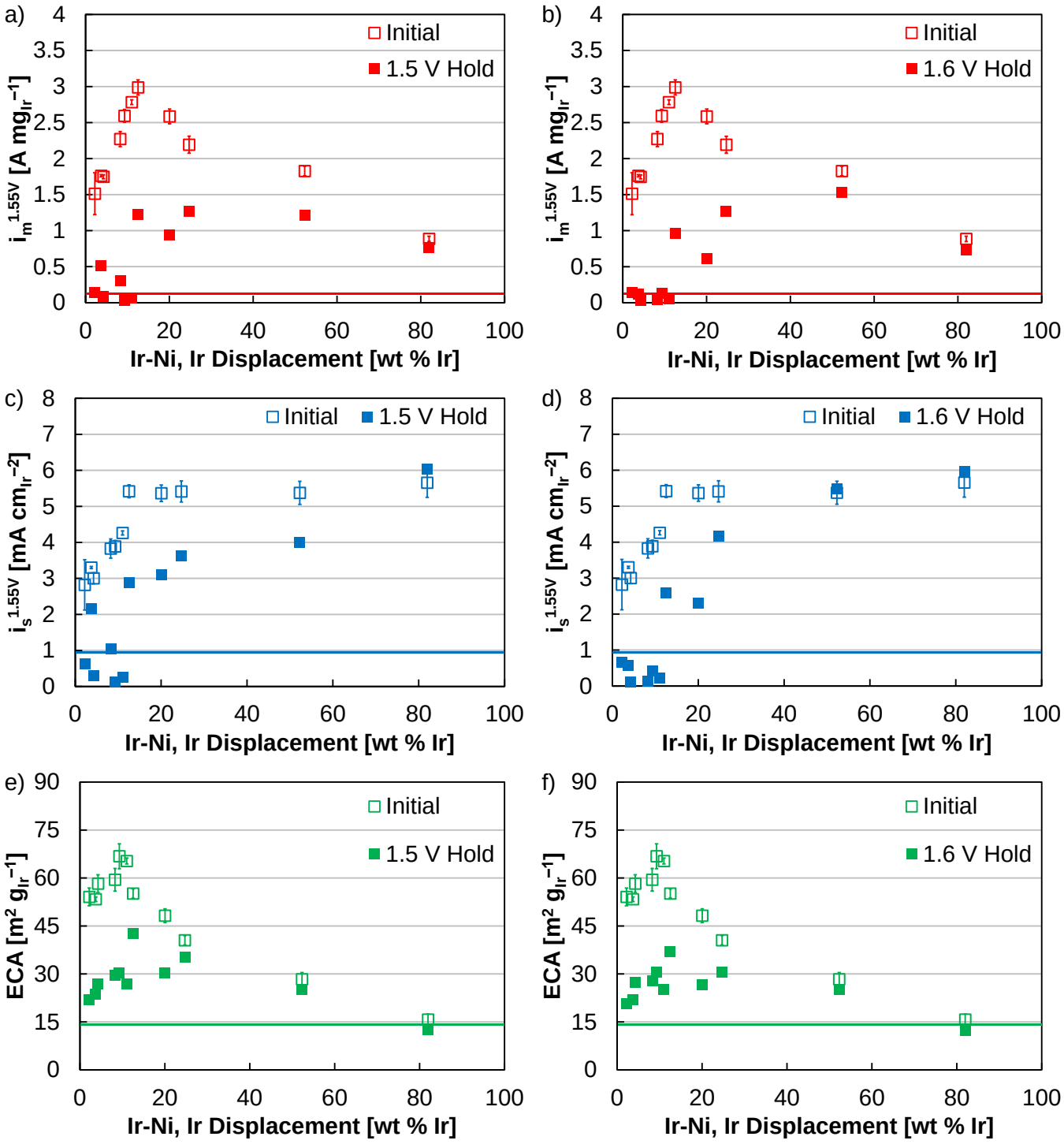

Figure S6. OER (a-b) mass activities, (c-d) specific activities, and (e-f) ECAs of as-synthesized Ir-Ni nanowires prior to and following durability, by potential holds at (a, c, e) 1.5 V and (b, d, f) 1.6 V vs. RHE. Horizontal lines indicate the mass activity, specific activity, and ECA of Ir nanoparticles following durability tests.

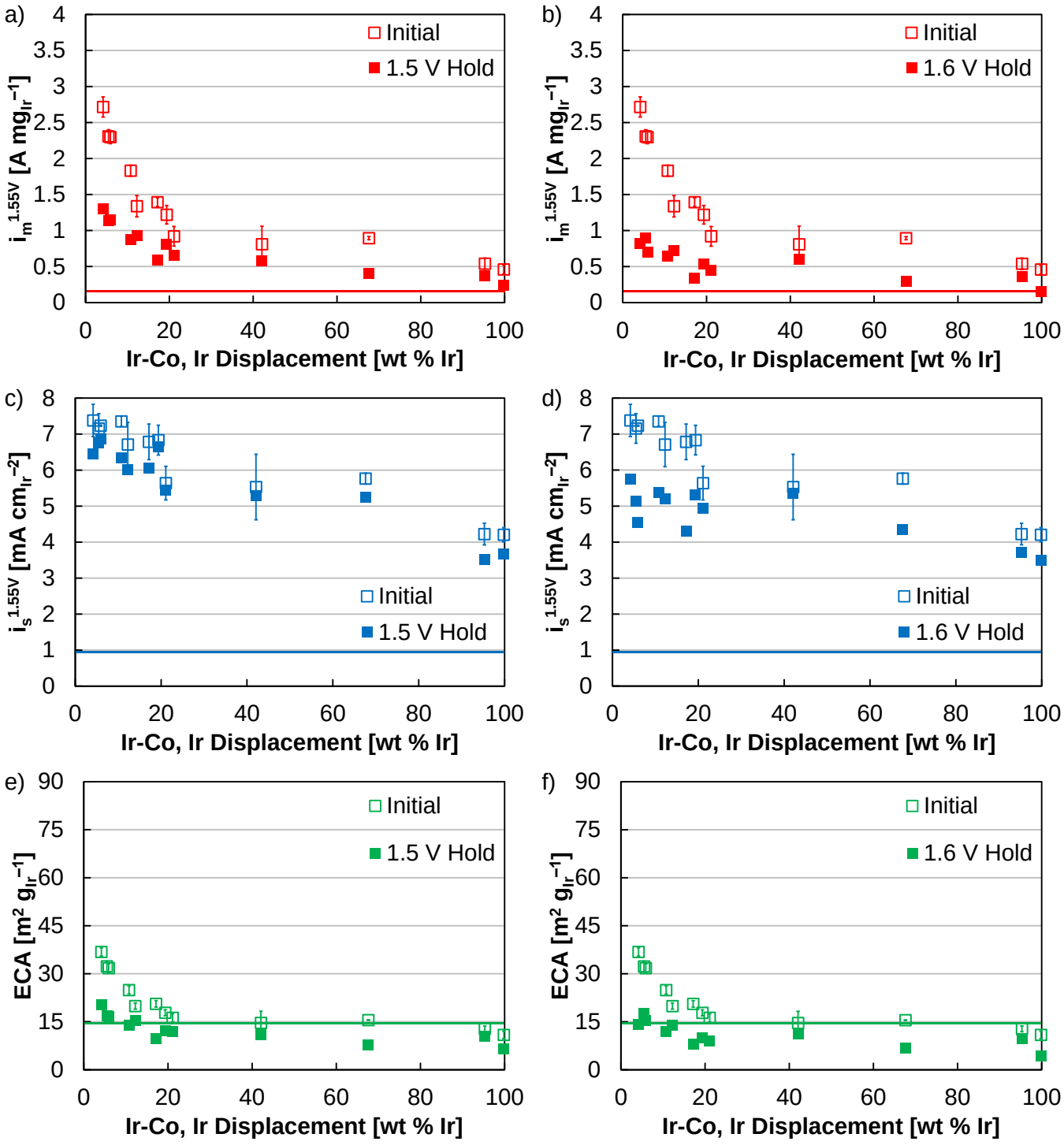

Figure S7. OER (a-b) mass activities, (c-d) specific activities, and (e-f) ECAs of as-synthesized Ir-Co nanowires prior to and following durability, by potential holds at (a, c, e) 1.5 V and (b, d, f) 1.6 V vs. RHE. Horizontal lines indicate the mass activity, specific activity, and ECA of Ir nanoparticles following durability tests.

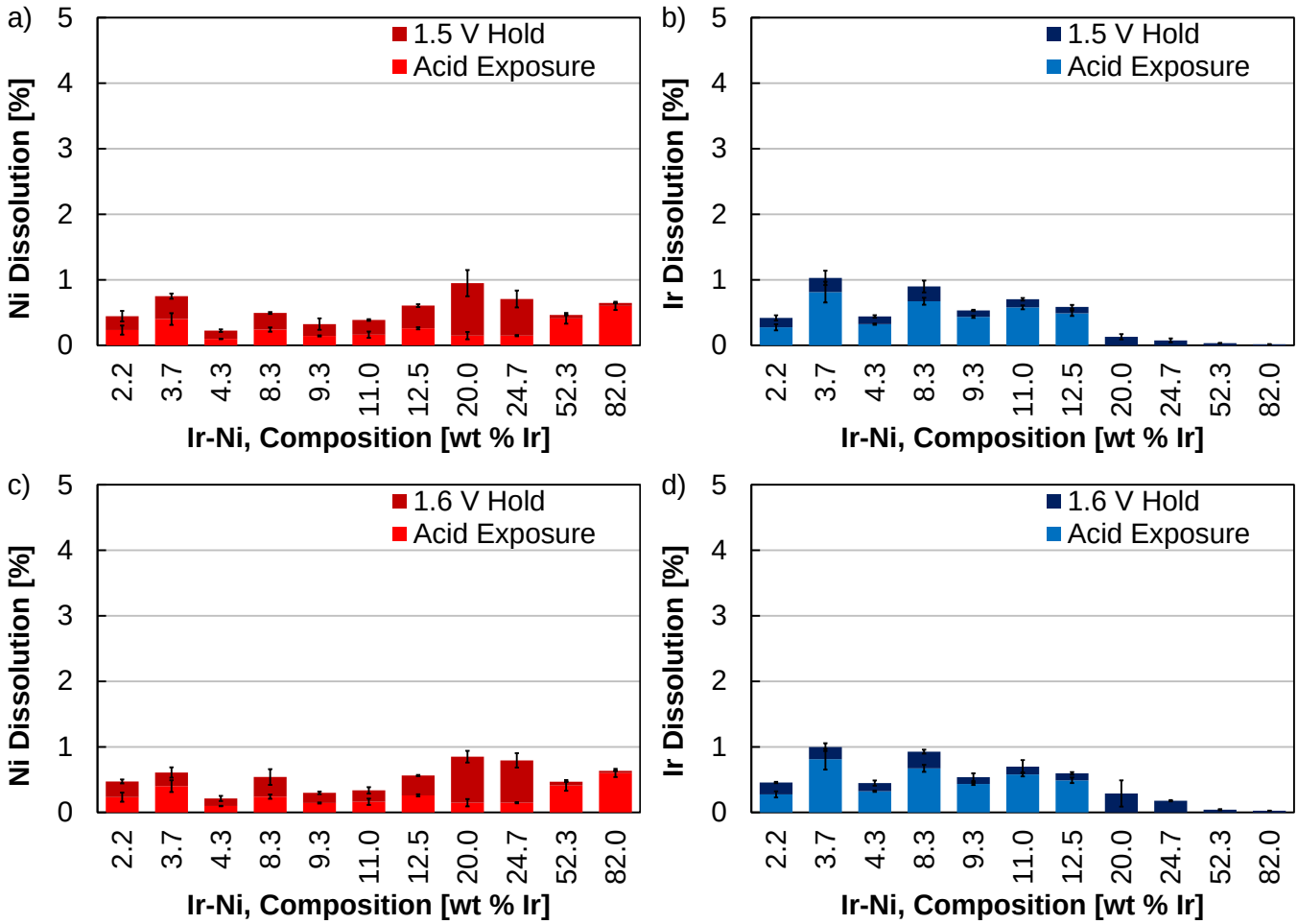

Figure S8. As-synthesized Ir-Ni nanowire dissolution into the electrolyte following electrochemical conditioning and durability tests at 1.5 V (a-b) and 1.6 V (c-d), with the nanowire composition listed on the x-axis (wt. % Ir).

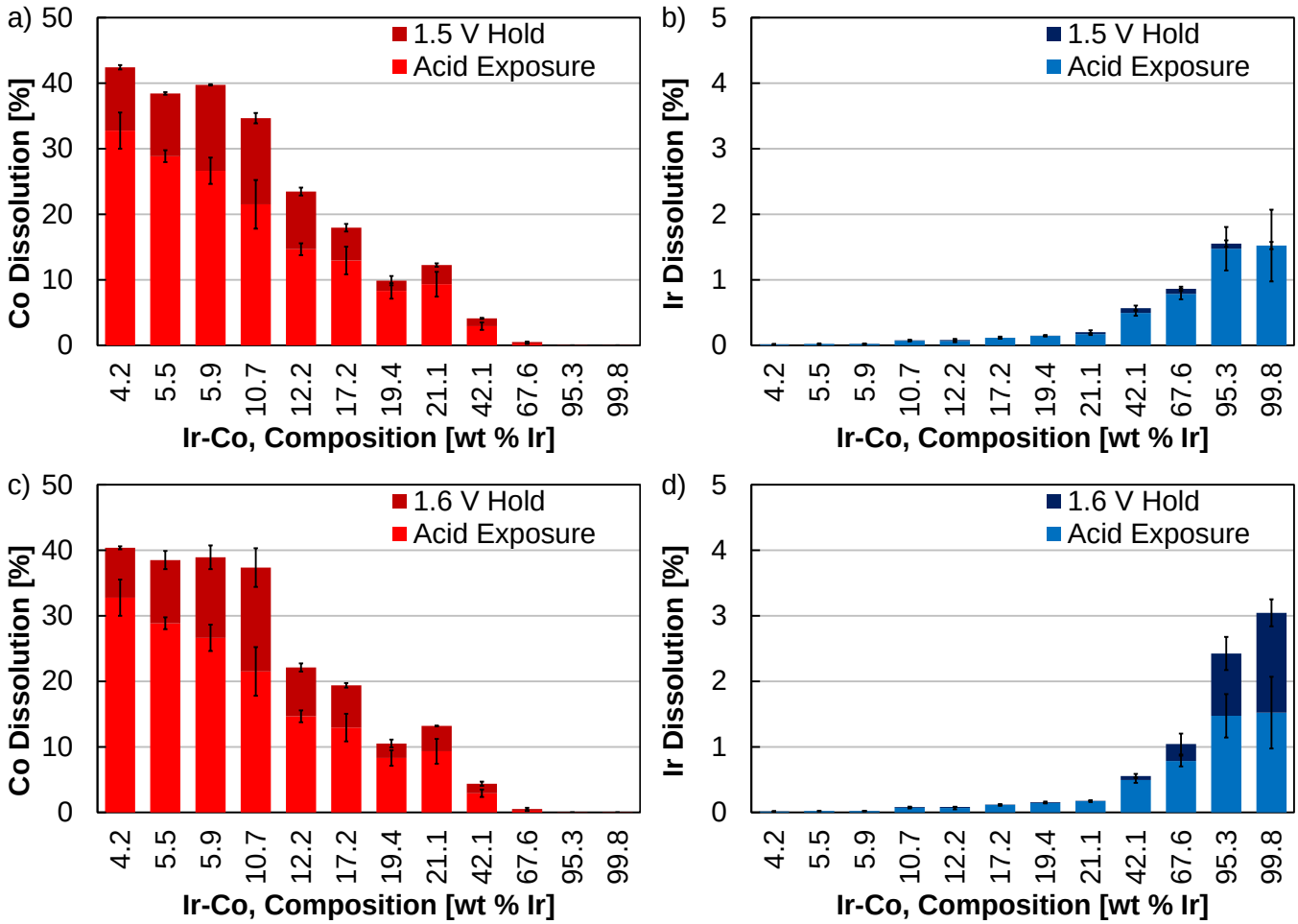

Figure S9. As-synthesized Ir-Co nanowire dissolution into the electrolyte following electrochemical conditioning and durability tests at 1.5 V (a-b) and 1.6 V (c-d), with the nanowire composition listed on the x-axis (wt. % Ir).

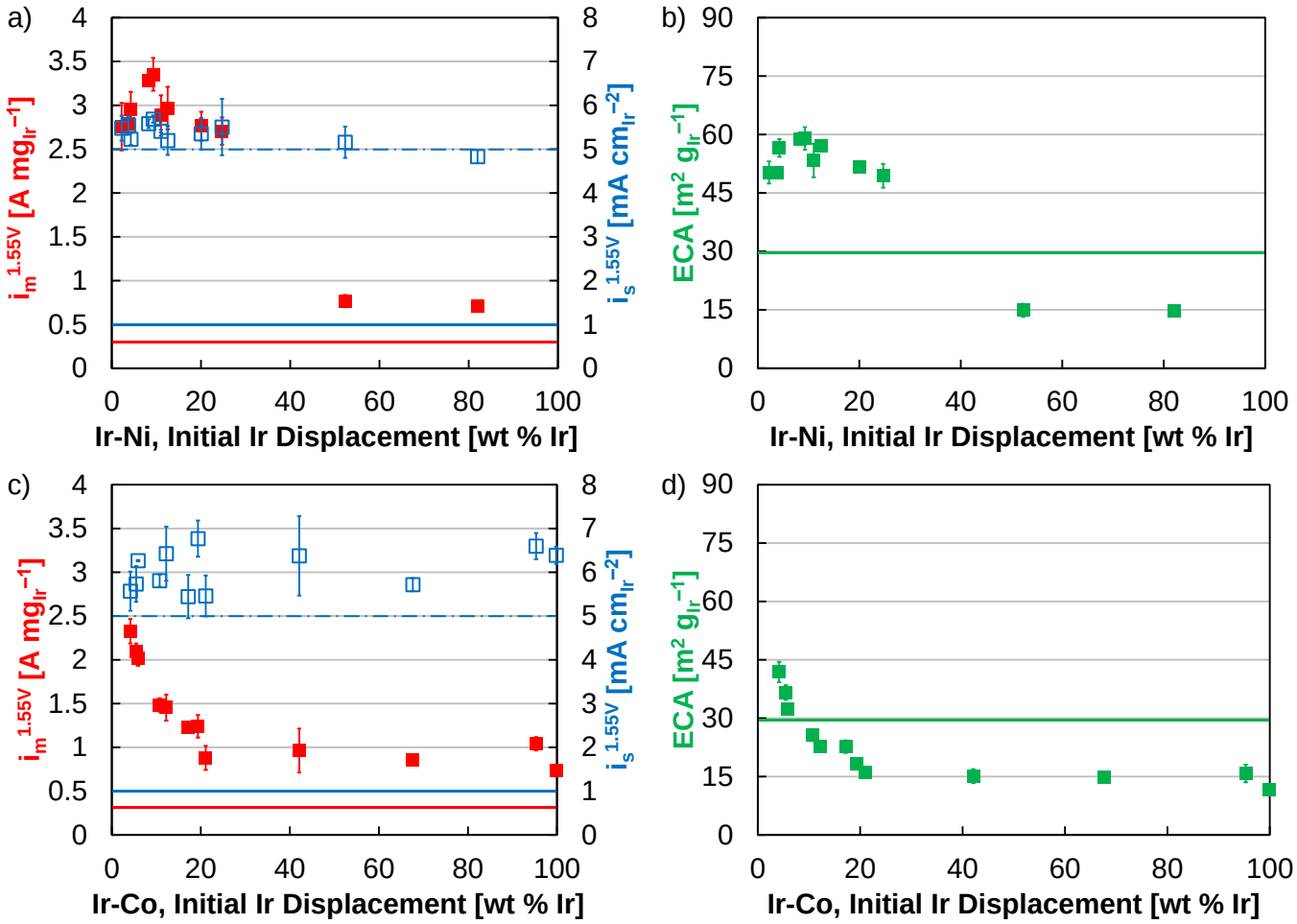

Figure S10. OER mass activities (red), specific activities (blue), and ECAs (green) of acid-leached (a-b) Ir-Ni and (c-d) Ir-Co nanowires. Following acid leaching, the composition of the nanowires are all greater than 90 wt. % Ir, but are plotted by the as-synthesized composition (x-axis) to discuss relevant data trends. Solid horizontal lines indicate the mass activity, specific activity, and ECA of Ir nanoparticles. Dashed horizontal lines indicate the specific activity of polycrystalline Ir.

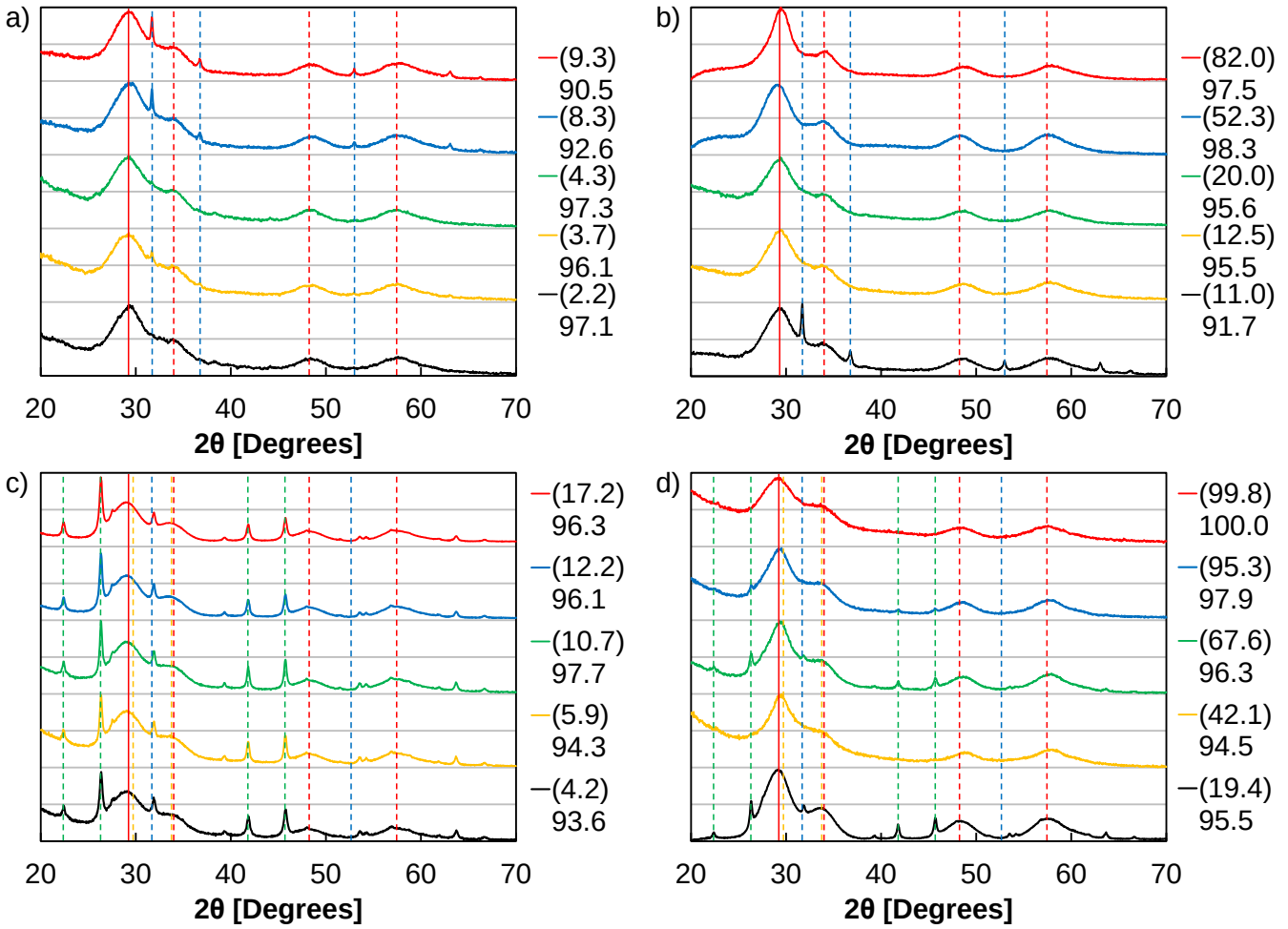

Figure S11. XRD patterns of (a-b) Ir-Ni and (c-d) Ir-Co nanowires following acid leaching with Ir composition (wt. % Ir) listed in the figure legends, as-synthesized in parentheses and following the acid leach. Vertical lines in (a-b) correspond to Ir fcc (red) and Ni fcc (blue). Vertical lines (c-f) correspond to Ir fcc (red), Co fcc (blue), Co_3O_4 monoclinic (green), and Co hcp (yellow). The solid red line (a-d) corresponds to the Ir fcc (111) peak.

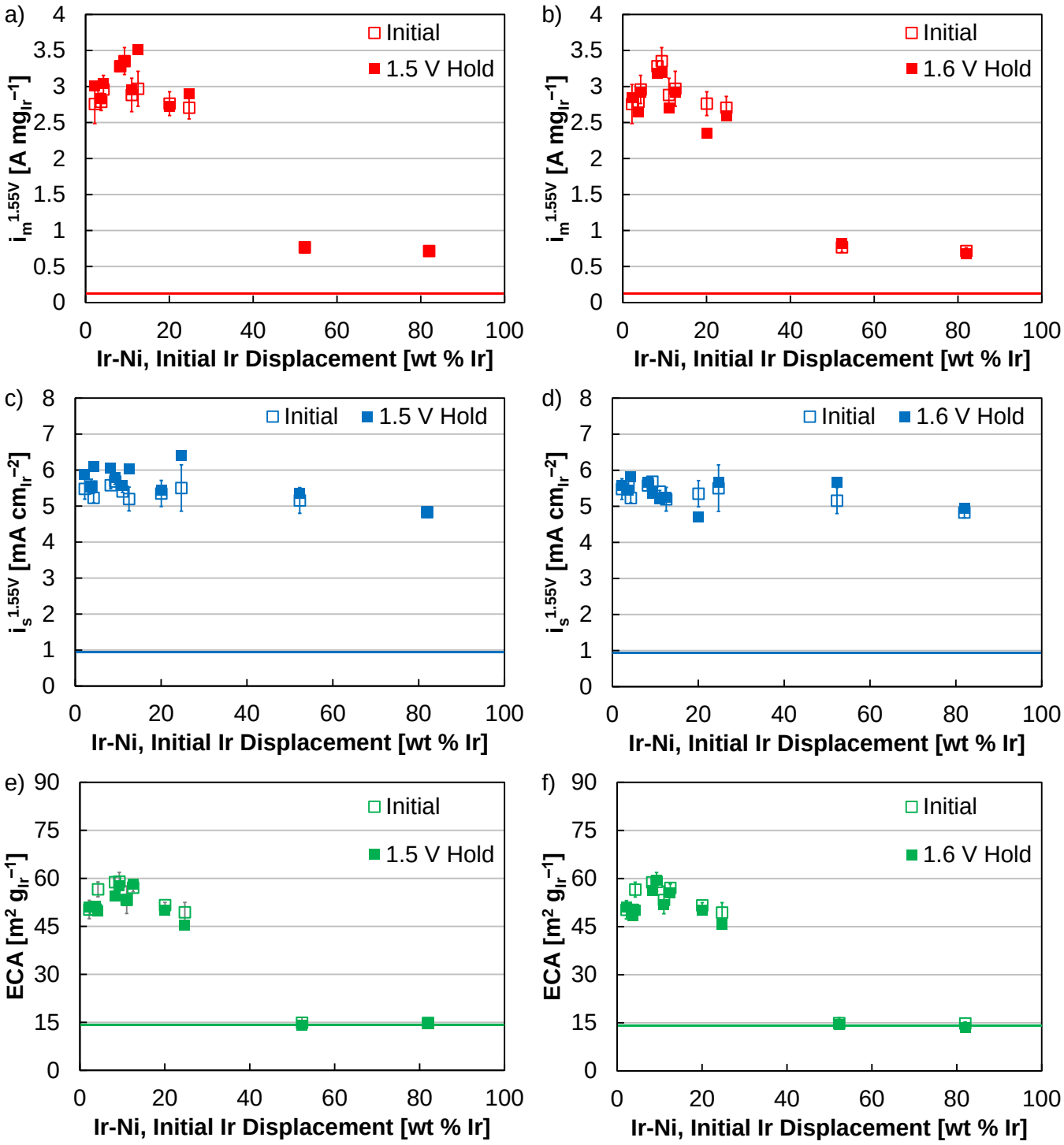

Figure S12. OER (a-b) mass activities, (c-d) specific activities, and (e-f) ECAs of acid leached Ir-Ni nanowires prior to and following durability, by potential holds at (a, c, e) 1.5 V and (b, d, f) 1.6 V vs. RHE. Following acid leaching, the composition of the nanowires were all greater than 90 wt. % Ir, but are plotted by the as-synthesized composition (x-axis) to discuss relevant data trends. Horizontal lines indicate the mass activity, specific activity, and ECA of Ir nanoparticles following durability tests.

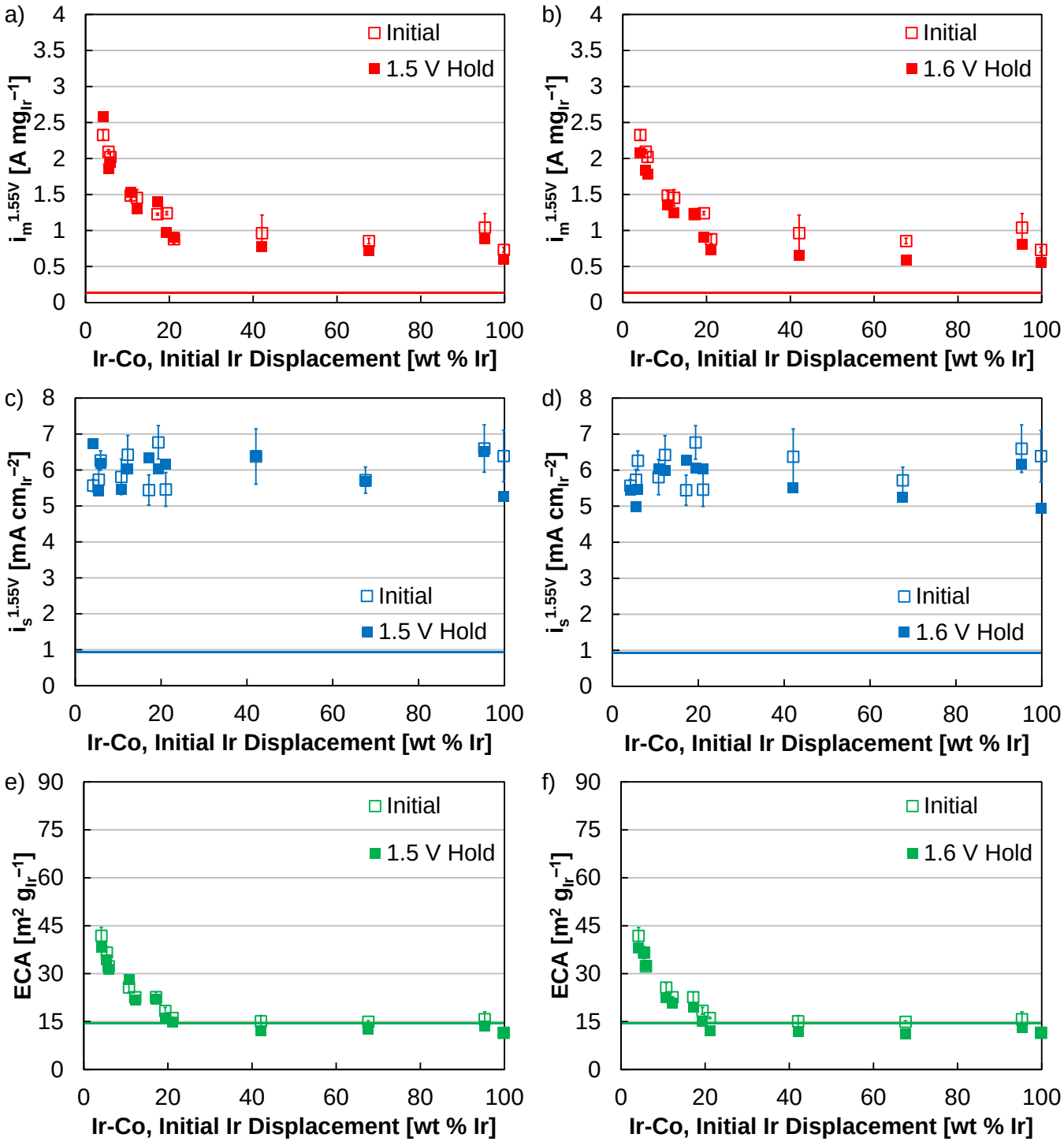

Figure S13. OER (a-b) mass activities, (c-d) specific activities, and (e-f) ECAs of acid leached Ir-Co nanowires prior to and following durability, by potential holds at (a, c, e) 1.5 V and (b, d, f) 1.6 V vs. RHE. Following acid leaching, the composition of the nanowires were all greater than 90 wt. % Ir, but are plotted by the as-synthesized composition (x-axis) to discuss relevant data trends. Horizontal lines indicate the mass activity, specific activity, and ECA of Ir nanoparticles following durability tests.

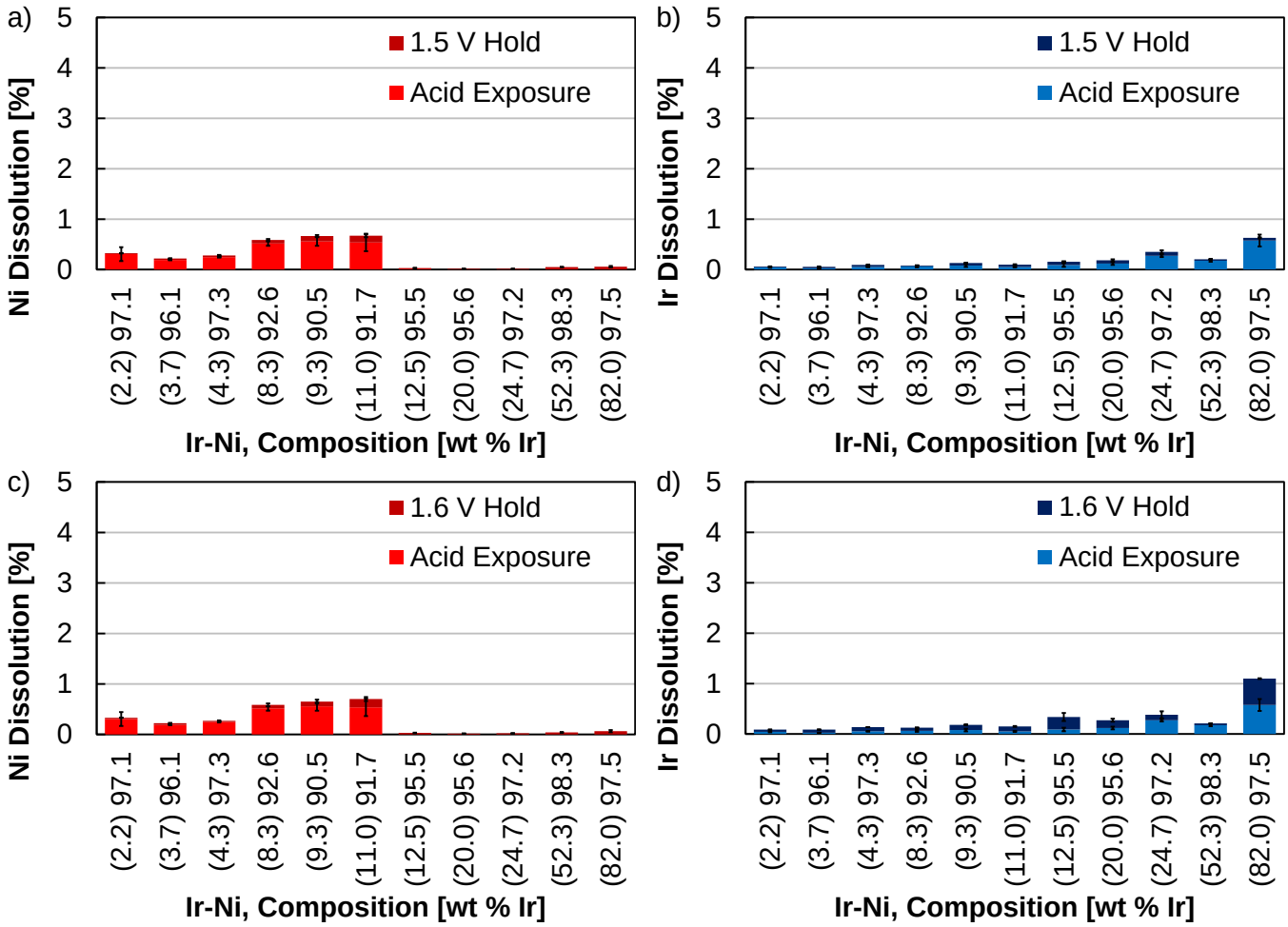

Figure S14. Acid leached Ir-Ni nanowire dissolution into the electrolyte following electrochemical conditioning and durability tests at 1.5 V (a-b) and 1.6 V (c-d), with the nanowire composition listed on the x-axis (wt. % Ir), as-synthesized in parentheses and following the acid leach.

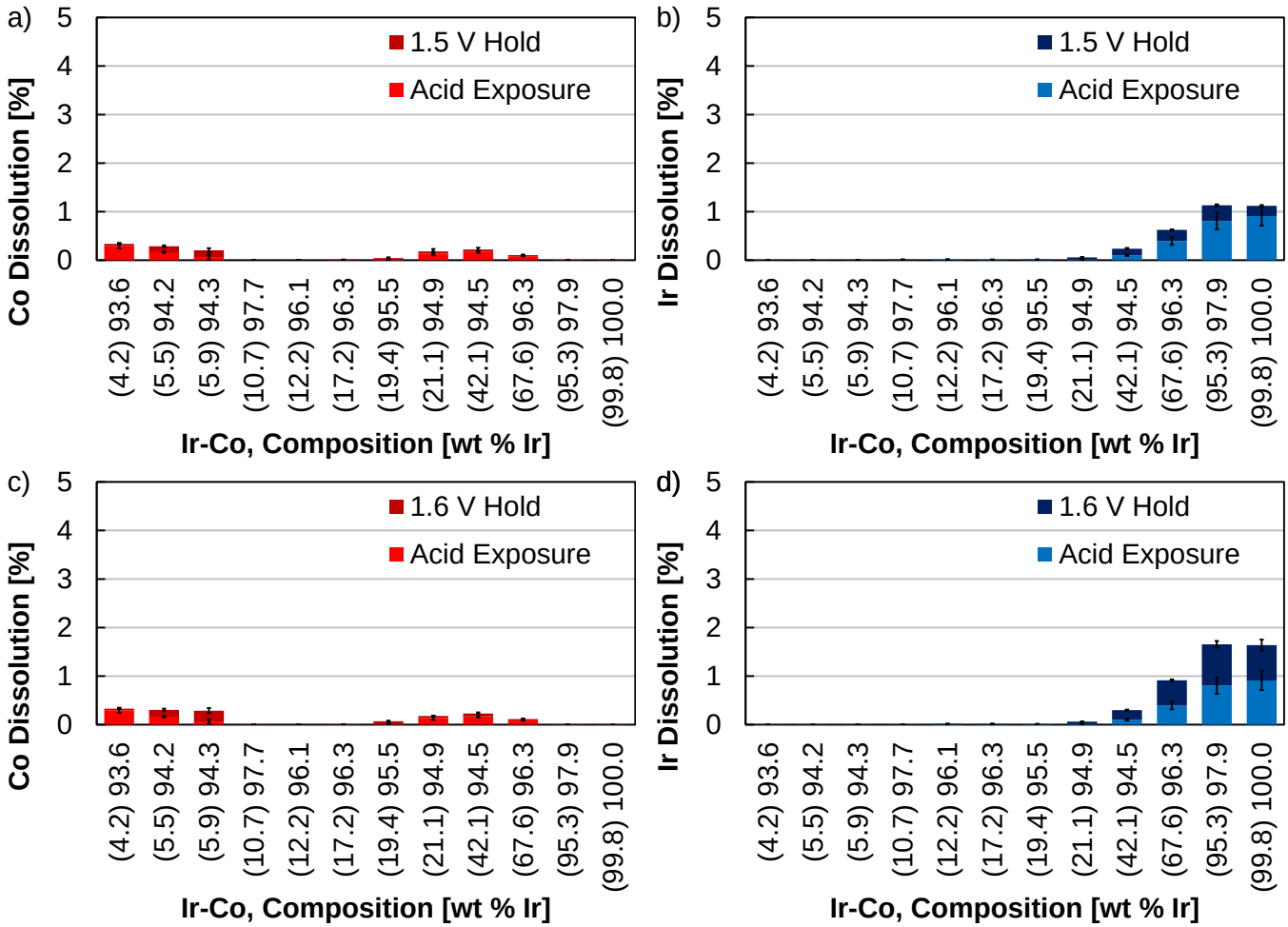

Figure S15. Acid leached Ir-Co nanowire dissolution into the electrolyte following electrochemical conditioning and durability tests at 1.5 V (a-b) and 1.6 V (c-d), with the nanowire composition listed on the x-axis (wt. % Ir), as-synthesized in parentheses and following the acid leach.

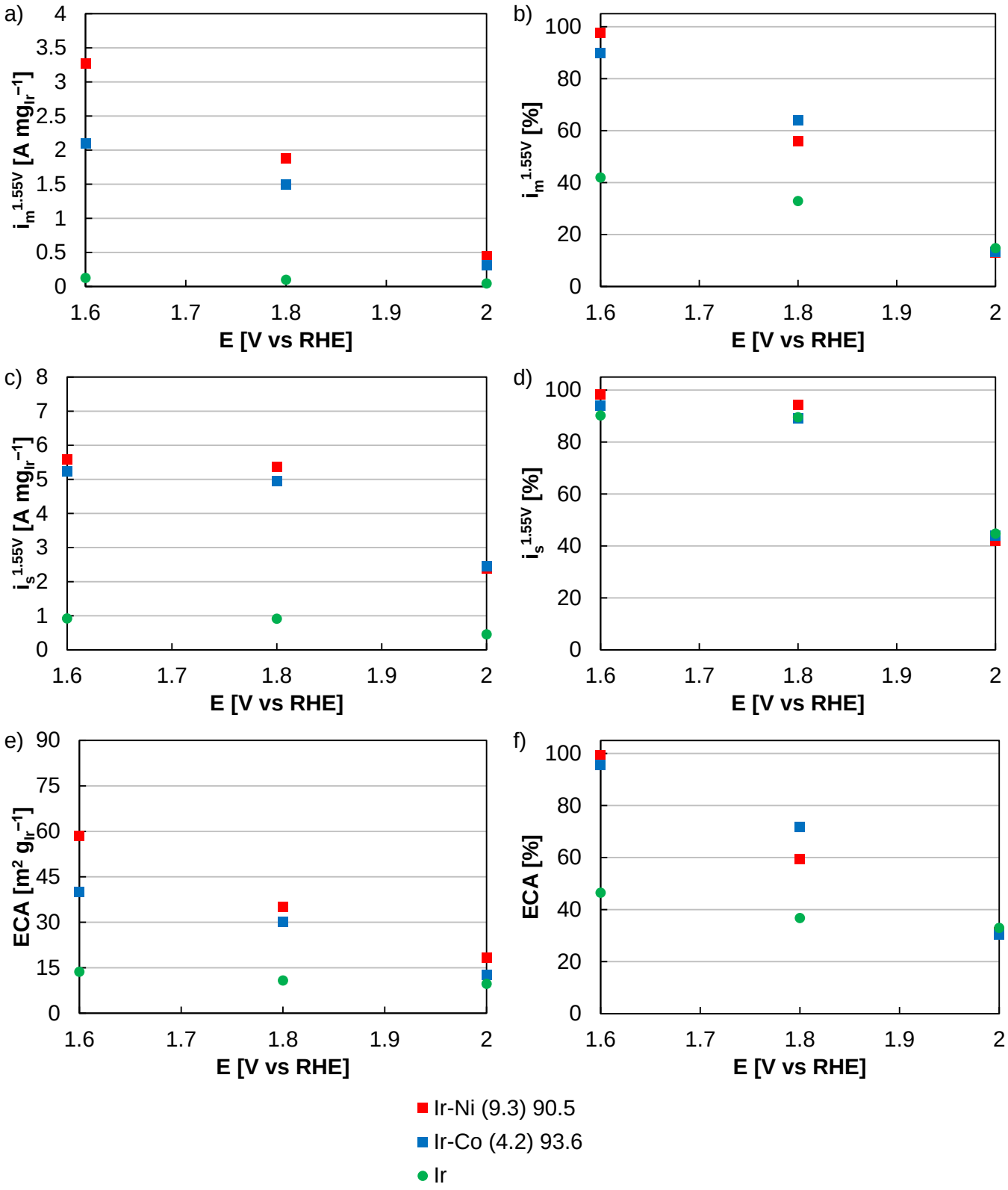

Figure S16. (a,b) OER mass activities, (c,d) OER specific activities, and (e,f) ECAs of acid leached Ir-Ni nanowires (Ir-Ni (9.3) 90.5, red), acid leached Ir-Co nanowires (Ir-Co (4.2) 93.6, blue), and Ir nanoparticles (Ir, green) after potential cycling durability tests. Data was presented as (a,c,e) actual values and (b,d,f) the percentage of the initial performance retained. Testing was completed by 30,000 cycles in the potential range of 1.4–1.6, 1.4–1.8, 1.4–2.0 V, with the upper potential specified on the x-axis. Scan rates during these tests were adjusted (1.4–1.6 V at 247 mV s^{-1}, 1.4–1.8 V at 494 mV s^{-1}, 1.4–2.0 V at 741 mV s^{-1}) to match the duration (13.5 h) of the potential hold durability tests.